University of Bristol - Explore Bristol Research
General rights

Case Study

Analysis of Fiber-Optic Strain-Monitoring Data from a Prestressed Concrete Bridge

G. T. Webb, Ph.D.[1]; P. J. Vardanega, Ph.D., M.ASCE[2]; N. A. Hoult, Ph.D., M.ASCE[3]; P. R. A. Fidler[4]; P. J. Bennett, Ph.D.[5]; and C. R. Middleton, Ph.D., C.Eng.[6]

Abstract: This paper presents data from fiber-optic strain monitoring of the Nine Wells Bridge, which is a three-span, pretensioned, prestressed concrete beam-and-slab bridge located in Cambridgeshire in the United Kingdom. The original deployment at the site and the challenges associated with collecting distributed strain data using the Brillouin optical time domain reflectometry (BOTDR) technique are described. In particular, construction and deployment issues of fiber robustness and temperature effects are highlighted. The challenges of interpreting the collected data as well as the potential value of information that may be obtained are discussed. Challenges involved with relating measurements to the expected levels of prestress, including the effects due to debonding, creep, and shrinkage, are discussed and analyzed. This paper provides an opportunity to study whether two commonly used models for creep and shrinkage, adequately model data collected in field conditions. **DOI: [10.1061/(ASCE)BE.1943-5592.0000996](https://doi.org/10.1061/(ASCE)BE.1943-5592.0000996).** *This work is made available under the terms of the Creative Commons Attribution 4.0 International license, http://creativecommons.org/licenses/by/4.0/.*

Author keywords: Brillouin optical time domain reflectometry (BOTDR); Concrete creep; Concrete shrinkage; Prestressed concrete; Structural health monitoring; Strain measurement.

Introduction

In 2008 a new road bridge was built to the south of the city of Cambridge in the United Kingdom. The Nine Wells Bridge provided an ideal test bed to trial new sensor and instrumentation technologies suitable for installation during construction. One such technology with the potential for embedment into a structure during construction uses fiber-optic sensors (Casas and Cruz 2003). Fiber-optic strain sensing is becoming more commonplace, for example, Costa and Figueires (2012) investigated deployment challenges when using fiber-optic technologies on a steel arch bridge in Portugal. Fiber-optic measurements have been proposed for corrosion detection (Wang and Huang 2011) and crack detection in concrete beams (Deif et al. 2010; Regier and Hoult 2014b). The use of fiber-optic cables to measure strain has been used as a structural health monitoring (SHM) technique for well over a decade

including embedment within prestressed concrete beams (Maaskant et al. 1997).

However, the vast majority of these trials have used a technology known as fiber Bragg gratings (FBGs) (Maaskant et al. 1997; Moyo et al. 2005; Gebremichael et al. 2005), which uses small gratings that act as localized "strain gauges" on a fiber-optic cable and have a resolution of the order of $1\ \mu\varepsilon$ (Gebremichael et al. 2005). Although it is possible to manufacture multiple FBG sensors along the same optical fiber, in order to distinguish between readings from each grating, each must be selected such that they all produce reflections at different frequencies over their entire strain range. This limits the number of strain gauges that may be present on a single fiber-optic cable.

Another technique for using fiber-optic cables to measure strain is Brillouin optical time domain reflectometry (BOTDR). In this approach light pulses are sent down a cable and the frequency spectrum of light that is reflected back, or backscattered, is measured (Parker et al. 1997). The peak frequency of the backscattered light spectrum is influenced by both the temperature and the strain in the fiber-optic cable (Kurashima et al. 1993). If the temperature is known, then the strain in the cable can be determined by subtracting the effects of temperature. Unfortunately the intensity of the backscattered light in BOTDR is very low compared with FBG, which means that many readings have to be taken and averaged together, resulting in increased measurement times and decreased accuracy. The random error produced by commercially available BOTDR analyzers is normally distributed with a standard deviation of approximately $15\ \mu\varepsilon$ (Klar et al. 2006).

In addition to the Brillouin effect, when a pulse of light is transmitted down a glass fiber a proportion of light is reflected due to variations in the refractive index of the fiber along its length. This is known as Rayleigh scattering. The intensity of this scattered light has been found to be proportional to strain, although like Brillouin scattering it is also sensitive to changes in temperature. With current commercially available analyzers, the technique can be used only with fibers of up to around 70 m in length, compared with

[1]Engineer, WSP | Parsons Brinckerhoff, 6 Devonshire Square, London EC2M 4YE, U.K. E-mail: graham.webb@cantab.net

[2]Lecturer in Civil Engineering, Dept. of Civil Engineering, Univ. of Bristol, Bristol BS8 1TR, U.K. (corresponding author). ORCID: http://orcid.org/0000-0001-7177-7851. E-mail: p.j.vardanega@bristol.ac.uk

[3]Associate Professor, Dept. of Civil Engineering, Queen's Univ., Kingston, ON, Canada K7L 3N6. E-mail: neil.hoult@queensu.ca

[4]Computer Associate, Dept. of Engineering, Univ. of Cambridge, Cambridge CB2 1PZ, U.K. E-mail: praf1@cam.ac.uk

[5]Formerly, Senior Research Associate, Dept. of Engineering, Univ. of Cambridge, Cambridge CB2 1PZ, U.K. E-mail: drpeterbennett@yahoo.co.uk

[6]Laing O'Rourke Professor of Construction Engineering, Dept. of Engineering, Univ. of Cambridge, Cambridge CB2 1PZ, U.K. E-mail: crm11@cam.ac.uk

the lengths of many kilometers that are possible with Brillouin scattering–based systems. Hoult et al. (2014), and Regier and Hoult (2014a) demonstrated the ability of Rayleigh scattering methods with fiber-optic sensors to measure distributed strains for bridge applications with improved spatial (5–20 mm) and strain (~1 $\mu\varepsilon$) resolution. Henault et al. (2012) demonstrated that these sensors could be used to measure concrete strain in beams tested in four-point bending to get results that were consistent with those obtained from vibrating wire strain gauges (VWSGs). Villalba and Casas (2013) used this technology as an early onset crack detection tool for reinforced concrete beams by using distributed strain measurements from fibers bonded to the surface of concrete beams. Michaud et al. (2016) used a Rayleigh-based system to characterize the differences in behavior between beams with and without recycled aggregate. The strain results were used to detect the development of cracks and corresponding increases in reinforcement strain at earlier loads for beams with high levels of aggregate replacement.

The BOTDR technique has been validated in a laboratory environment for prestressed concrete beams by researchers such as Gao et al. (2006) and Zhou et al. (2009). Klar et al. (2006) and Bourne-Webb et al. (2009) performed investigations involving an embedded fiber BOTDR system in a field trial for piling work. In this case the fiber-optic cables were installed in piles at a test site and a commercial development site prior to construction. Field trials have also been performed by Zhang et al. (2007) on a prestressed concrete box girder and Matta et al. (2008) on a steel structure; however, these studies have focused on externally bonded fiber-optic cables.

Ge et al. (2014) performed a laboratory study comparing VWSGs, FBGs, and BOTDR embedded in reinforced concrete beams and concluded that a significant difference is seen between the sensor types (up to 25–30%). There is a need for further field trials using the BOTDR technique on bridge structures, especially using fibers that are embedded during construction (rather than externally attached). Distributed monitoring techniques, such as BOTDR, have a number of advantages over systems that provide only discrete point measurements. Because measurements are taken at every location along the cable, there is a much lower chance of any localized issues on the structure not being detected.

According to Ghali et al. (2016), "…codes do not have adequate provisions that specify controllable means for safety against serviceability failure; examples are the means to control the harmful effects of creep and shrinkage of concrete, relaxation of prestressed steel, temperature variations, and prestress loss." Howells et al. (2005) studied the sensitivity of many creep and shrinkage models for concrete and concluded that the relative humidity and compressive strength of the concrete are highly influential. Lark et al. (2004) studied long-term creep and shrinkage performance (over 16 years) of two posttensioned bridges and showed that some common design approaches gave reasonable agreement with the measured field data (albeit conservatively). This paper provides an excellent opportunity to study the match (or lack thereof) of two creep and shrinkage prediction models for prestressed concrete (CEN 2004; Collins and Mitchell 1997) using field measurements.

System Deployment

The Nine Wells Bridge (Fig. 1) in Cambridgeshire, U.K., is a three-span bridge that carries a new road over the main rail line connecting Cambridge to London. Construction began in the summer of 2008 and was completed in the summer of 2009. Each bridge span is approximately 30 m long and consists of 12 precast prestressed concrete beams (Fig. 2) supported on laminated rubber bearings.

Each beam has 27×15.2-mm-diameter prestressing strands along the bottom chord and 4×15.2-mm-diameter strands along the top chord (Fig. 3). Each of the prestressing strands was
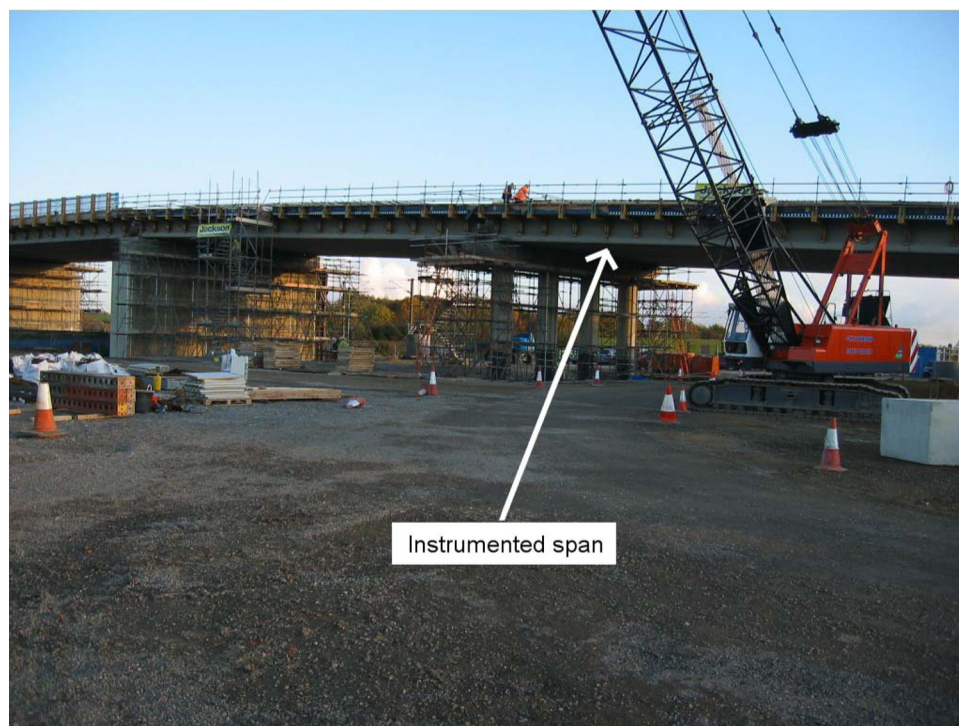

Fig. 1. (Color) Nine Wells Bridge during construction (image by N. A. Hoult)
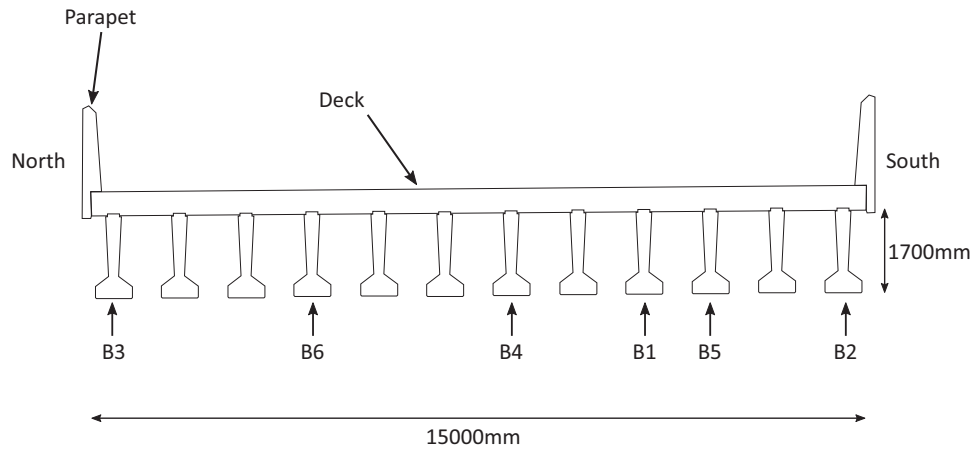
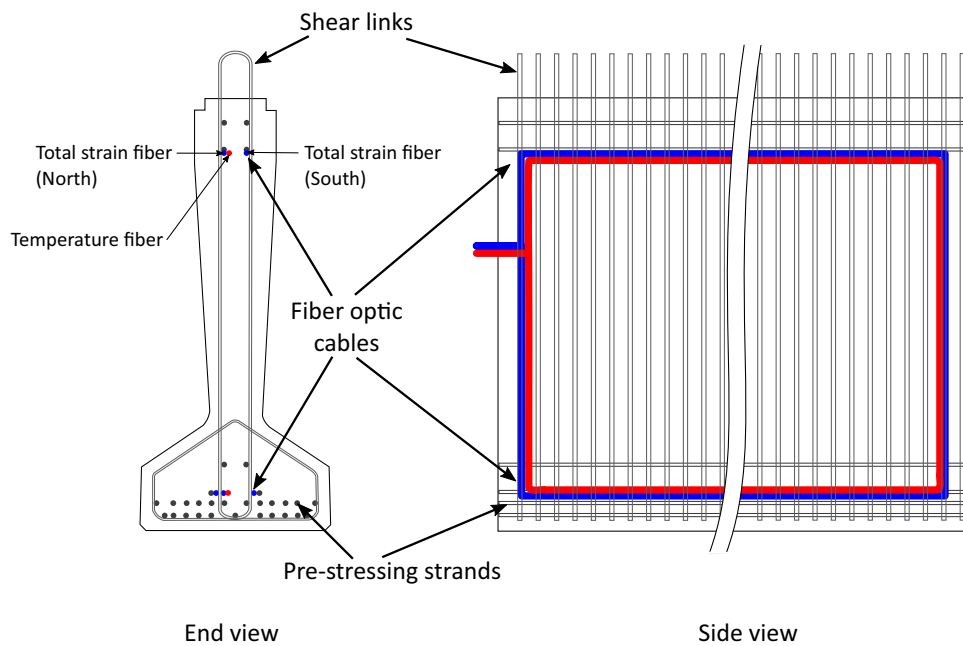**Fig. 2.** Bridge cross section indicating instrumented beams

Fig. 3. (Color) Beam cross section showing fiber-optic cable locations (adapted from Hoult et al. 2009)

pretensioned to 162 kN, which was 70% of the 232-kN characteristic breaking strength. The deck slab, which was cast in situ, is 294 mm thick with 25-mm-diameter longitudinal reinforcement bars at the top and 20-mm-diameter bars at the bottom, both at 150-mm spacing. The nominal concrete cover was specified as 40 mm. The beams were designed to be initially simply supported before being made continuous over the two intermediate piers when the in situ deck slab was cast (as shown in the sketch in Fig. 4 and the photograph presented as Fig. 5). This research project was undertaken to explore the potential capabilities of using the BOTDR technique on bridge structures in addition to examining the practical challenges faced by such deployments. Some details of the deployment have been discussed in Hoult et al. (2009) and also briefly in Vardanega et al. (2016a, b). A full treatment of the project is presented in this case study. This bridge was also used as part of a separate research project

examining the potential of using vibration monitoring of structures as a characterization and damage-detection tool (Whelan et al. 2010).

Purpose of Monitoring

The ability to collect data is not sufficient for any monitoring system to yield valuable information. Webb et al. (2014b) presented a classification system for SHM deployments, which can be classified as (1) sensor deployment studies, (2) anomaly detection, (3) model validation, (4) threshold check, or (5) damage detection. This classification system will be used to describe aspects of the deployment in this paper.

In addition to trialing a relatively new sensing technique (sensor deployment study), the monitoring installation also aimed to provide value to the designers/owners of the bridge. Measuring strains would

allow the long-term behavior of the structure to be analyzed. There was interest in comparing these measurements to various empirical creep and shrinkage models (model validation). Finally, the ways in which this system could potentially be used for damage detection were considered.

Description of Monitoring

Six beams in the western-most span, denoted B1–B6, were instrumented as illustrated in Fig. 2. The fiber-optic cables were installed in each beam at the precasting yard after the prestressing strands had been pretensioned but before steel reinforcing stirrups had been tied in place in the mold. Two types of fiber-optic cables (Fig. 6) were installed in the six beams, one bonded to the concrete (hereafter referred to as the total strain fiber) and one in which the sensing core was not bonded to the concrete (hereafter referred to as the temperature fiber). The cables used to measure temperature strain consisted of optical fibers suspended in a gel, which prevented shear transfer between the concrete and the sensing core, encased in a protective coating. These cables [Fig. 7(a)] were 6 mm in diameter but were only glued to the prestressing strands at the ends of the beam and supported every few meters by tape. As such there was room for the concrete to penetrate between the cable and the prestressing strand reducing any potential effects the fiber-optic cable would have on the prestressing bond. This allows the effects of temperature on the Brillouin frequency shift to be removed, such that the true strain in the total strain fiber (due to applied loading as well as time-dependent effects and the thermal response of the structure) can be calculated. The fiber-optic cables used to measure total strain were low-cost (regular telecommunications grade) cables except for one beam (Specimen B4). The low-cost cable was a 12-core ribbon cable ($\sim 0.3 \times 3.2$ mm) as shown in Figs. 6 and 7(b). This provided sufficient surface area to bond with the concrete while at the same time not interfering with the bond between the prestressing strands and the concrete. In Specimen B4, a single, more robust, fiber-optic ribbon cable [Fig. 7(c)] with a reinforced protective sheath was installed along one of the top strands to compare the performance of these more expensive cables with the low-cost telecommunications grade cables. This cable consisted of 4 glass cores with cladding embedded in a nylon sleeve with steel wires running down each edge of the sleeve either side of the four cores. This cable was approximately 5 mm wide and 1 mm thick and, as with the other two cables, it was only glued to the strand at the ends and supported intermittently to minimize the influence the cable would have on the bond. The bottom cables in all beams were low-cost telecommunications grade 12-core ribbon.

The fibers were installed as a loop within each beam, as illustrated in Fig. 3. Each beam had a single fiber-optic cable for temperature measurement installed in this way. In Beams B1, B2, B5, and B6 two fiber-optic cables for total strain measurement were installed on either side of the cross section, hereafter referred to as the north and south fibers (Fig. 3). Because of time constraints, only one total strain measurement cable was installed in Beam B3. In Beam B4, as previously mentioned, a more robust fiber-optic cable was used along the top strand with a telecommunications grade 12-core ribbon cable used along the bottom. Each total strain measurement cable was installed with an initial pretension to ensure that the cable would not go into compression due to the applied loading or creep in the concrete.

Deployment Time Line

Table 1 gives the dates on which measurements were taken from Beams B1 and B6, as well as key dates in the bridge's construction process. Readings were taken from the north fiber along the bottom of Beam B1 and along both the bottom and top of Beam B6. Fibers in the remaining beams were unable to provide any data due to the robustness issues discussed next.

System Operation

Robustness Issues

One of the aims of this monitoring campaign was to determine whether standard low-cost telecommunications grade fiber-optic cables could reliably be used to measure strains in concrete beams. Unfortunately, a number of these cables were damaged, both during the casting and installation of the beams. Fig. 8 shows the location of the fiber-optic cables in the mold prior to casting and Fig. 9 shows the completed beams. The cables proved to be highly susceptible to breakage during the pouring and vibration of the concrete, and as a result a number of cables were snapped during the casting process. Other fibers were damaged while the beams were transported from the precasting yard to the bridge site and lifted into position. After the beams had been cast, it was found that only half of the total number of fiber-optic cables that had originally been installed (11 of 21) remained intact. However, following transport and erection on site, this figure had fallen to just under one-third (6 of 21), meaning several beams were left with no functioning fibers at all. This figure had reduced to 14% (3 of 21) 314 days after installation, although readings were still possible along the bottom of Beam B1 and along the top and bottom of Beam B6.

At the bridge site, additional fiber-optic cables were spliced to those entering each beam and the fibers fed down through metal protective ducts from the ends of the beams to metal boxes mounted on the face of the bridge abutment at ground level to provide access to the fibers when taking readings. Standard telecommunications grade fibers were used for all beams because the metal ducts and boxes were intended to provide sufficient protection; however, the fibers were susceptible to damage during the construction process. The metal boxes were also vandalized on a number of occasions, damaging more of the fibers. By 2009 all the remaining fibers within Beam B6 had become unusable. Clearly, the inexpensive telecommunications grade fibers are not sufficiently robust to be installed in concrete structures. However, even if the more expensive, durable fibers had been used throughout, the total cost of installing the monitoring system would still have only been of the order of 1% of the total cost of the bridge. If the system could provide useful information to the owners of the bridge, then this cost might be considered a worthwhile investment.

Raw Data

The BOTDR analyzer produces, for each fiber connected to it, a data file consisting of raw strain values (positive values indicate tension) averaged over a 1-m gauge length, taken every 50 mm along the fiber. Postprocessing is required to turn these raw values into usable strain readings. Fig. 10 shows some plots of the raw strain output for Beam B1. [Raw strain data is presented for Beam B1 and Beam B6 in beam-1-data.xlsx and beam-6-data.xlsx (Webb et al. 2016)]. Each line shows data taken from a different measurement time and shows several features. In each data set there is a large strain change at the point in which the fibers enter the beam. Because the length of the fiber outside the beam was not known beforehand, this allows the spatial location of readings inside the beam to be determined. This fiber also had to be repaired following damage due to vandalism. The resulting
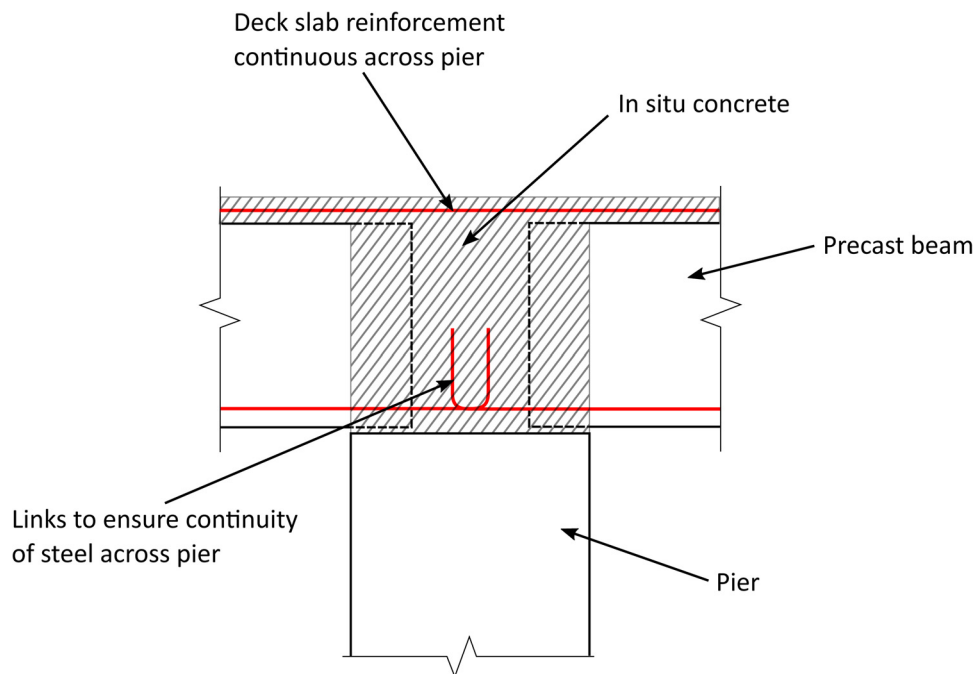
Fig. 4. (Color) Indicative sketch showing the beam continuity detail

Fig. 5. (Color) Continuity of bridge beams (image by N. A. Hoult)

change in fiber length can clearly be observed in the plot (Fig. 10). A shift can be applied to the data sets following the repair to ensure that this length change does not affect results. It is important to note that any individual set of readings cannot be interpreted to give the strain in the concrete because they depend on the original reference values of strain taken when the fiber was attached to the prestressing tendon prior to construction of the beam. Instead, the relative changes in values between readings taken at different times are related to the changes in concrete strain. The apparent changes in strain visible at a distance of around 36 m do not, therefore, represent a variation in strain in the concrete.

Temperature Compensation

Raw strain readings from the analyzer (denoted ζ in the following discussion) are affected by temperature in two ways. When the glass fiber changes temperature the total strain will vary due to thermal expansion, which can be estimated using the thermal coefficient of the fiber, α_f. In addition there is a coefficient of temperature-induced apparent strain, α_a, which allows for the temperature dependency of the Brillouin effect. Adding these two effects gives a combined thermal expansion coefficient for the temperature fibers, which relates the change in temperature, ΔT, to the change in the raw strain as measured by the analyzer, $\Delta \zeta_t$, given in

$$\Delta \zeta_t = (\alpha_f + \alpha_a)\Delta T \qquad (1)$$

For the cables used in this installation, $\alpha_f = 4.2 \times 10^{-6}/°C$ and $\alpha_a = 19.471 \times 10^{-6}/°C$ (values from Mohamad 2008). Table 2 shows the average change in temperature since the initial set of readings, for each reading from Beam B1. The initial set of readings was taken shortly after the concrete had been poured, when significant temperature rises are caused by the exothermic hydration reaction of the setting cement. This explains why subsequent data sets have large negative differential temperatures.

Because the strain fiber is bonded to the concrete beam, it is assumed that it will experience the same mechanical strain changes as the surrounding concrete, $\Delta \varepsilon_c$, in addition to a temperature-
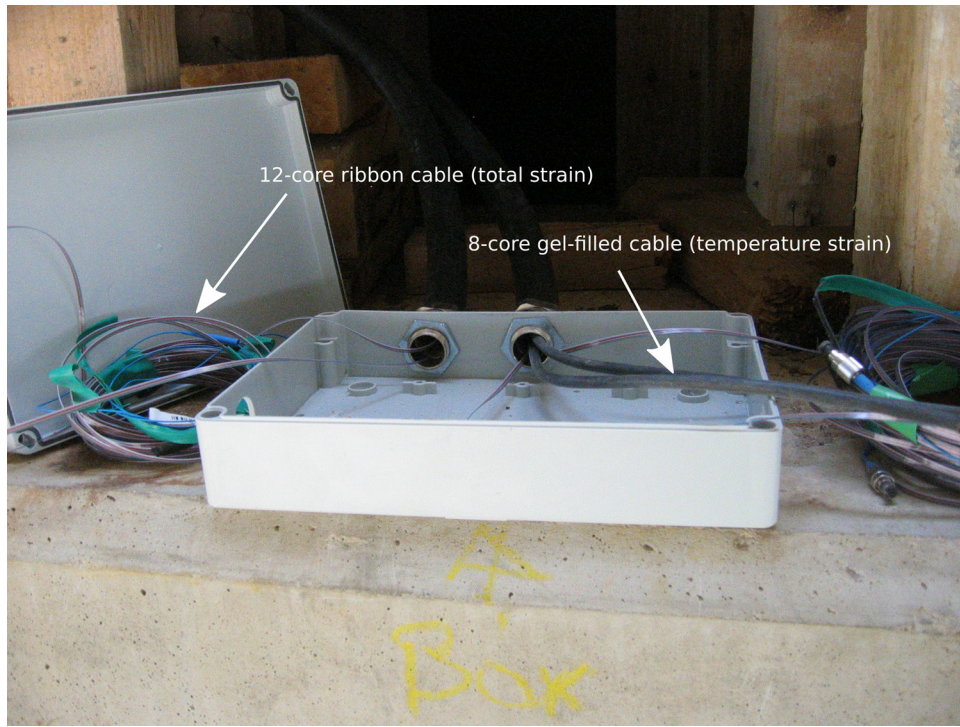
Fig. 6. (Color) Total strain and temperature strain fiber-optic cables routed to a junction box during installation (image by N. A. Hoult)
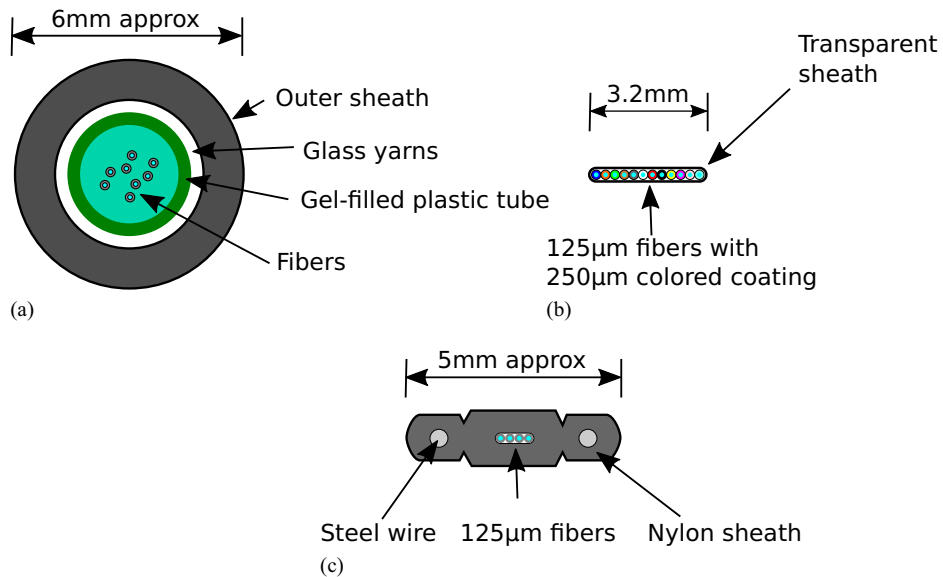

Fig. 7. (Color) Cross sections of the fiber-optic cables used in the deployment (adapted from Mohamad 2008): (a) Excel 8-core loose tube cable; (b) 12-core ribbon cable; (c) Fujikura reinforced 4-core ribbon cable

induced apparent strain, giving a change in raw strain as measured by the analyzer, $\Delta \zeta_s$, given in

$$\Delta \zeta_s = \Delta \varepsilon_c + \alpha_a \Delta T \qquad (2)$$

Eqs. (1) and (2) can be combined to give an expression for the actual change in the mechanical strain in the concrete as calculated using

$$\Delta \varepsilon_c = \Delta \zeta_s - \frac{\alpha_a}{\alpha_a + \alpha_f} \Delta \zeta_t \qquad (3)$$

This concrete strain will be a combination of strains due to thermal expansion of the concrete, creep and shrinkage effects, and any loads applied to the beam after the initial set of baseline readings, such as prestressing force and the addition of the in situ deck slab. Live loads are usually temporary loads, but they can be measured using this system if applied for more than the 20 min required to

Table 1. Summary of Strain Measurement Dates for Beams B1 and B6

Date	Beam B1 Cast: 07/29/08 Released: 07/30/08	Beam B6 Cast: 08/21/08 Released: 08/23/08
07/30/08	Before release	—
07/30/08	After release	—
07/30/08	After demolding	—
07/31/08	Day 1	—
08/08/08	Day 9	—
08/29/08	Day 30	Day 6
10/08/08	—	Day 40
10/10/08	Day 72	—
11/24/08	Day 117 (after deck added)	Day 93 (after deck added)
06/09/09	Day 314	Day 284
12/02/09	Day 491	Fiber broken
03/10/11	Day 954	—
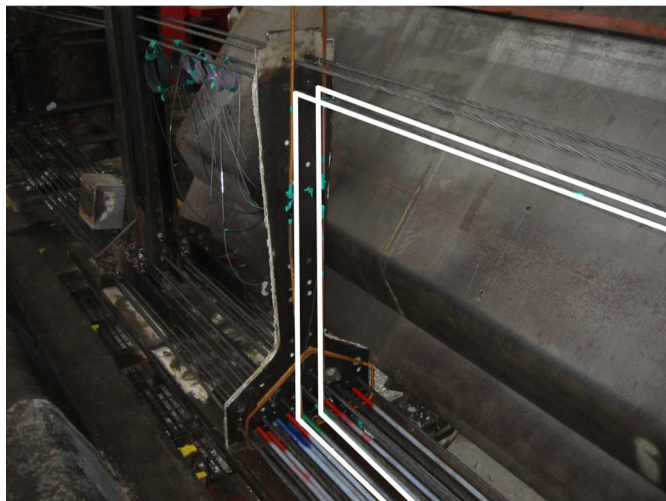
Fig. 8. (Color) Beam prestressing tendons prior to casting (with fiber-optic cable locations shown in white overlay) (image by N. A. Hoult)

Fig. 9. (Color) Beams after fabrication (image by N. A. Hoult)
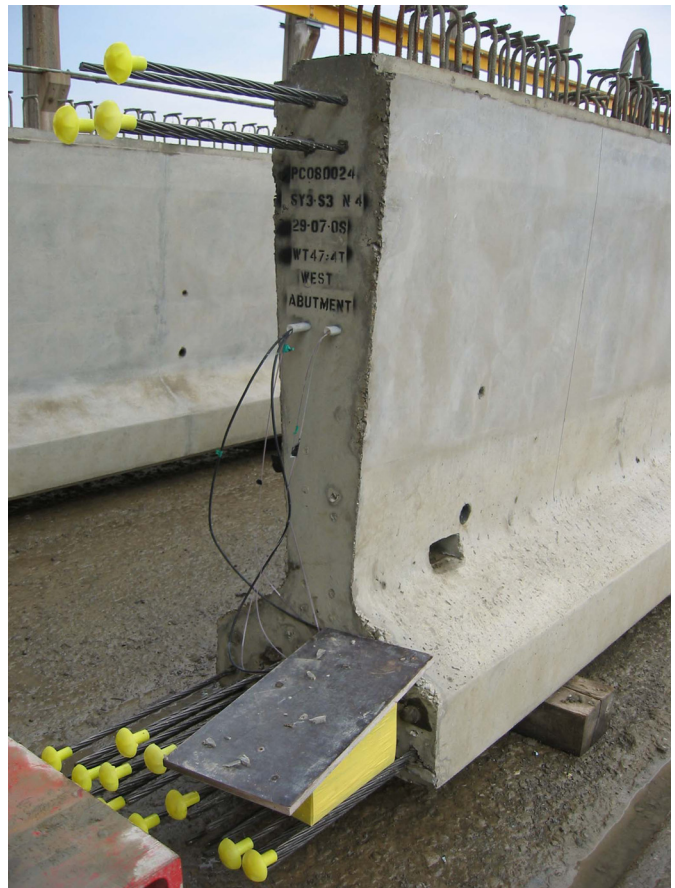
take a reading (e.g., a truck parked on a bridge). The strain change due to any load that is applied for significantly less than the scan time will not be measured correctly.

Data Interpretation

Sensor Deployment Study

There are a number of important factors to be considered when characterizing the performance of a new sensing technique. In addition to system reliability and robustness, which were discussed in the previous section, it is also important to consider the achievable accuracy.

Fig. 11 shows the strain readings obtained from the BOTDR analyzer, which exhibit a significant degree of apparent noise (scatter of up to 100 $\mu\varepsilon$). This is a characteristic of the BOTDR method. Whether this level of accuracy is acceptable or not depends on the intended application of the data, as will be discussed later. In addition to limiting the accuracy of measurements, this also means that the temperature correction calculation cannot simply be performed point by point along the beam, because the error due to scatter would be amplified in the compensated readings. Fig. 12 shows a moving average line (with a period of 2 m) applied to each set of

data to represent the important features of each data set, while compensating for the noise. The period of the moving average line needs to be chosen manually depending on the expected strain distribution being measured; if strains are expected to vary over a short length scale, then a moving average line with a small period will be required.

Because one of the primary aims of this monitoring was to investigate the long-term behavior of the bridge due to creep and shrinkage, it would be desirable to completely remove the effects of temperature from each reading. During the earlier stages of the bridge's construction the concrete beams could be treated as determinate structures; hence, the strains due to thermal expansions could be predicted. However, when the bridge becomes fully composite and continuous over all three spans, the indeterminacy of the structure makes it harder to predict strains. This therefore makes it difficult to separate the effects of temperature from those due to creep and shrinkage when analyzing the measured strains. This will be discussed in more detail later in the paper.

Model Validation

Because one of the aims of this research was to investigate the long-term behavior of the structure and validate the structural analysis models used for design, it was necessary to predict the expected development of strain over time to allow comparisons to be made with each set of readings. There were various changes to the loading applied to the beams during construction, and these had to be taken into consideration. Because the precast bridge beams were constructed from prestressed concrete, creep
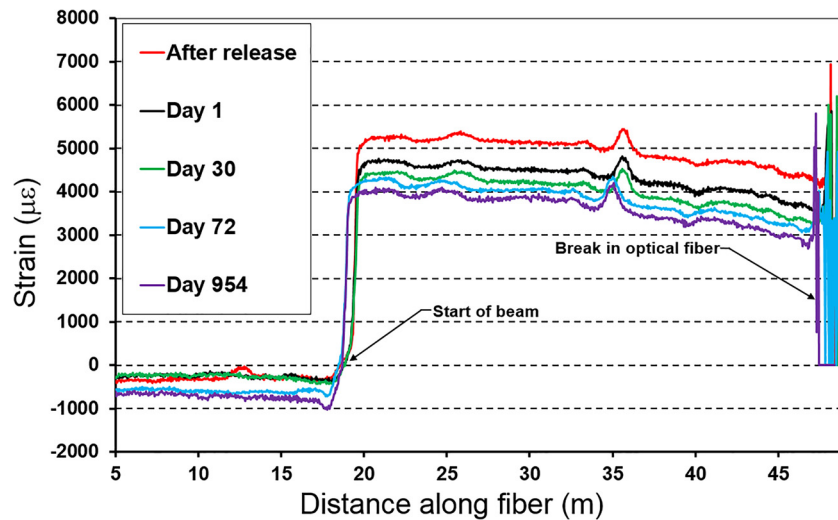
Fig. 10. (Color) Raw strain plot for Beam B1 north fiber; each line represents a reading taken at a different time

Table 2. Average Temperature Change with Time in Beam B1

Date	Temperature change (°C)
07/30/08	−8
07/31/08	−20
08/08/08	−28
08/29/08	−26
10/10/08	−33
11/24/08	−42
03/10/09	−35
06/09/09	−33
12/02/09	−41
03/10/11	−36

and shrinkage of the concrete were important factors to consider. Once the in situ deck slab was cast, the beams and deck began acting as a composite section and the bridge became continuous over the three spans, changing the behavior. The behavior of the concrete and steel tendons led to losses of prestressing force, which resulted in both short- and long-term effects. The material and beam properties used in the analysis are listed in Table 3.

Short-Term Effects

Releasing the prestressing tendons applies a large internal force within the concrete beam, which is balanced by a force in the concrete resulting in an internal moment, causing the beam to elastically deform. As the prestressing tendons are bonded to the concrete, the resulting shortening causes a loss of prestressing force, which is calculated as follows. The initial applied force, $P_0(x)$, and the eccentricity at which it is applied, $e(x)$, vary with distance, x, along the length of the beam due to some of the tendons being debonded using plastic tubing at each end of the beam. Because the prestressing tendons are concentrated in the lower part of the beam, a hogging bending moment will be induced, causing the center of the beam to lift off the ground. The beam will then behave as a simply supported beam with a uniformly distributed self-weight, which must be considered. The bending moment at a distance x along the beam for $x = 0$ to L is given by

$$M(x) = P_0(x)e(x) + \frac{wx^2}{2} - \frac{wLx}{2} \qquad (4)$$

where w = self-weight of the beam per unit length; and L = overall length of the beam. At a given cross section, at distance x along the length of the beam, the strain at any distance y from the centroid can then be found using

$$\varepsilon(x,y) = \frac{M(x)y}{E_cI_c} + \frac{P_0(x)}{A_cE_c} \qquad (5)$$

where E_c = Young's modulus of the concrete; I_c = second moment of area of the beam section; and A_c = beam's cross-sectional area. The force that remains present in the prestressing tendons, $P_1(x)$, can then be calculated from

$$P_1(x) = P_0(x) + A_s(x)E_s\varepsilon(x,e) \qquad (6)$$

where E_s = Young's modulus of steel; and $A_s(x)$ = cross-sectional area of the steel tendons effective at a distance x from the end of the beam. Because the prestressing force has now changed, the bending moment and axial force applied to the beam will also have changed, meaning Eqs. (4)–(6) should be iterated several times to converge to the new values for the prestressing force throughout the beam. Eq. (5) can then be used to calculate the strains expected in the fiber-optic cables attached to the upper and lower tendons in the beam. These predicted strains are shown in Fig. 13. The step changes in predicted strain at the locations in which tendons are debonded at each end of the beam can clearly be seen. Fig. 13 also shows measured data from the bottom fiber of Beam B1, taken immediately after the beam was removed from formwork. It can be seen that, for much of the beam, there is some visual agreement between the measured and predicted values, in particular the step changes in strain can be identified.

Long-Term Effects

There are three main long-term effects that lead to losses of prestressing force and, hence, strains: relaxation of steel, shrinkage of concrete, and creep of concrete. Because these effects depend on a number of variables that often cannot be determined with certainty, empirical relationships are normally used in predictions. In the
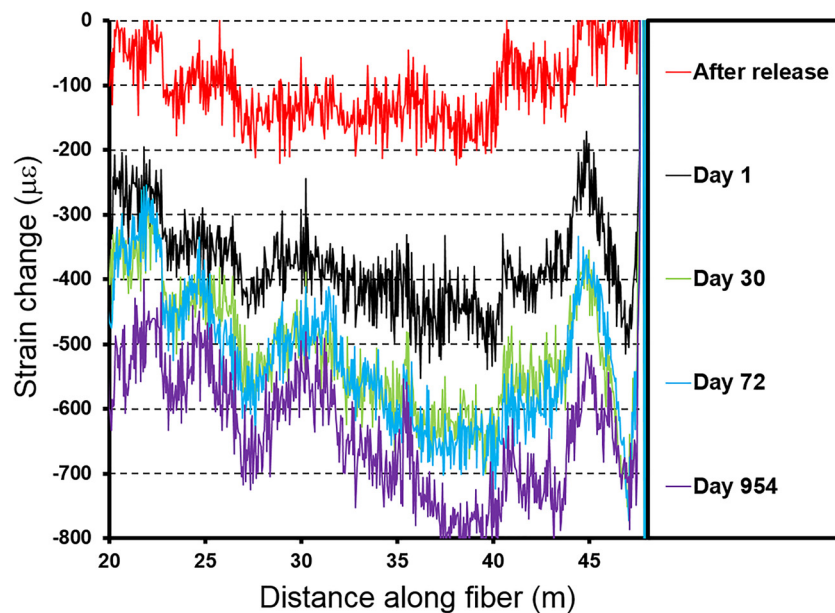
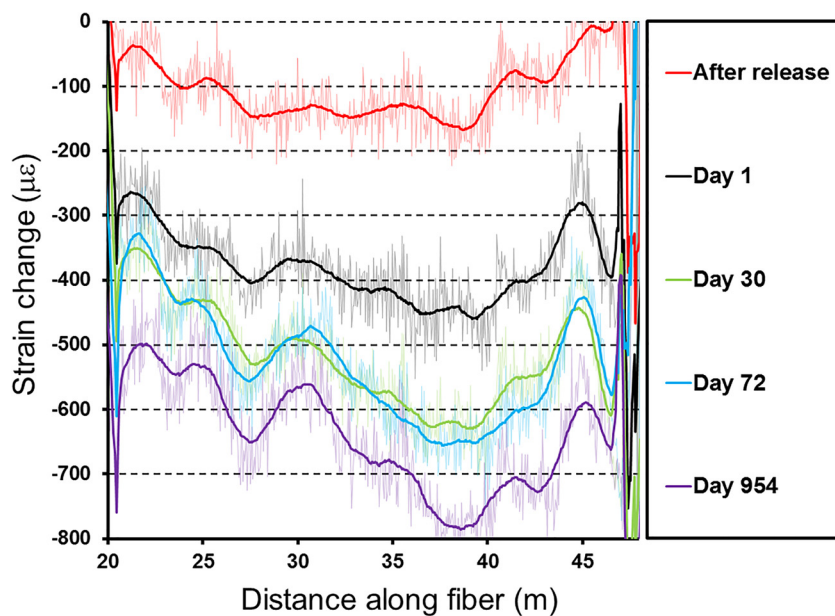**Fig. 11.** (Color) Strain plot for Beam B1 north fiber

Fig. 12. (Color) Strain plot for Beam B1 north fiber with moving average trend line

supplemental data (Appendices S1–S4) the detailed calculations for the effects of prestress relaxation, concrete shrinkage, and creep of concrete are set out in detail for both the approach given in Eurocode 2 (CEN 2004) (in Section S1) and Collins and Mitchell (1997) (in Section S2). The effects of the deck becoming a composite section (Section S3) and continuous beam analysis (Section S4) are also presented. Further details are also reported in Webb (2010, 2014). The effects of any longitudinal restraint provided by the elastomeric bearings have been assumed negligible when considering strains due to long-term effects such as creep and shrinkage or thermal actions.

Figs. 14–16 show predicted midspan strains using both the approach suggested by Collins and Mitchell (1997) and Eurocode 2 (CEN 2004) and measured midspan strains in Beams B1 (bottom),

B6 (top), and B6 (bottom), respectively. All strains are compressive due to the prestressing force applied to the beam. The majority of creep and shrinkage occurs in the early stages of the beam's life. The step change in strain when the in situ deck is added (on Day 117 for Beam B1 and Day 93 for Beam B6) can clearly be seen, as can its effect on further altering the creep response due to changes in the stress distribution in the beam. The predictions based on Eurocode 2 (CEN 2004) compare fairly well with those based on Collins and Mitchell (1997). The maximum discrepancy between the two calculation methods is around 100 $\mu\varepsilon$, which seems reasonable given the uncertainty involved in creep and shrinkage calculations.

In the measured data the effects of temperature have been considered by assuming that the beams can exhibit unrestrained thermal

expansions and contractions. Although this is a valid assumption in the initial stages of the bridge's construction, once the bridge becomes continuous over all three spans this assumption breaks down because the degree of restraint at each support is not known. The discrepancy between measured and predicted values would therefore be expected to be larger after the point in time when the bridge in situ deck slab was added and continuity between spans was achieved.

For Beam B1 (Fig. 14) there appears to be a good visual agreement between measured and predicted values. For both the measured and predicted values considered, for the majority of readings the difference is within the expected error due to noise (e.g., around 100 $\mu\varepsilon$ for the fiber optics). The discrepancy on Day 491 is larger, which could partly be due to the ambient temperature in December, which was 5–6°C cooler than most of the other measurement dates. In an unrestrained concrete beam this would cause an additional compressive strain of around 60 $\mu\varepsilon$. In the

continuous beam (the beams are partially restrained against thermal contraction due to being continuous) this strain would be resisted; hence, the data from Day 491 would be expected to have a lower magnitude of compressive strain than predicted, as can be seen in Fig. 14.

Beam B6 (Figs. 15 and 16) initially shows good visual agreement between measured and predicted values for both top and bottom fibers in the beam. However, even though the readings on Day 93 were taken after the deck had been added, the expected step changes in strain appear to be missing. Furthermore, there has been very little further change in strain in either the top or bottom of the beam in the readings following this date. Although the discrepancies between measured and predicted values in the bottom of the beam are within the expected error range, those from the top of the beam are not. This suggests that either this beam is behaving different from expectations, or there is a problem with the sensors in this beam. Because the fibers in this beam were found to have broken for subsequent readings, it is possible that by Day 284 they had already partially fractured.

Damage Detection

A commonly cited long-term aim for monitoring systems is to provide information to assist with the detection of damage or deterioration more effectively than relying solely on visual inspections. If using a discrete strain measurement system, then there is the possibility of damage occurring between individual point sensors and not being detected. A distributed strain monitoring system, such as BOTDR, does not have this limitation and therefore is particularly attractive.

One potential aim of this monitoring system could be to detect wire breaks within the prestressing tendons. Individual wire breaks within prestressing tendons cause minute changes in strain (less than 1 $\mu\varepsilon$) (Webb et al. 2014a). Because this magnitude of strain is far smaller than the accuracy and precision of BOTDR measurements, individual wire breaks will not be detected. However, Hoult et al. (2009) proposed that if an entire prestressing strand were to
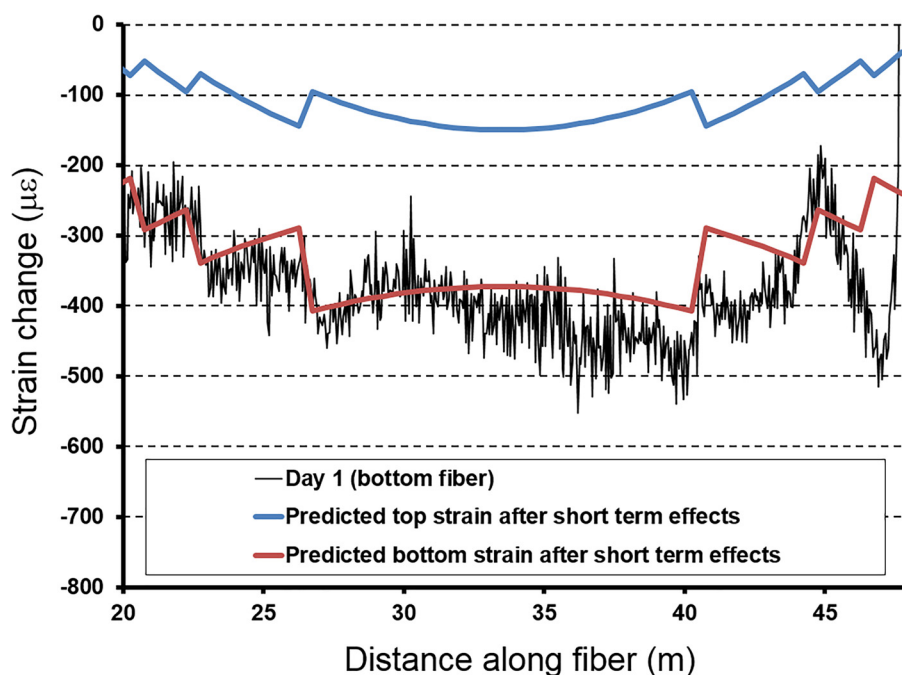
Table 3. Material and Beam Parameters Used for Analysis (Relevant Values Taken from or Derived from the As-Built Drawings)

Parameter	Symbol	Value
Young's modulus of steel	E_s	200 GPa
Characteristic tensile strength of steel	f_{pk}	1,860 MPa
Young's modulus of concrete	E_c	37 GPa
Characteristic concrete cylinder strength	f_{ck}	50 MPa
Area of prestressing steel	A_s	4,650 mm^2
Area of precast concrete (beams)	A_p	0.61 m^2
Area of in situ concrete (deck beams)	A_i	0.50 m^2
Second moment of area of precast concrete	I_p	1.76×10^{11} mm^4
Second moment of area of in situ concrete deck	I_i	5.87×10^9 mm^4
Initial prestressing force	P_0	6,092 kN
Eccentricity of prestressing force	e	411 mm
Self-weight of beam	w	14.71 kN/m
Length of perimeter exposed to drying	u	4,762 mm
Relative humidity	RH	80%

Fig. 13. (Color) Predicted and measured strains immediately after release for Beam B1
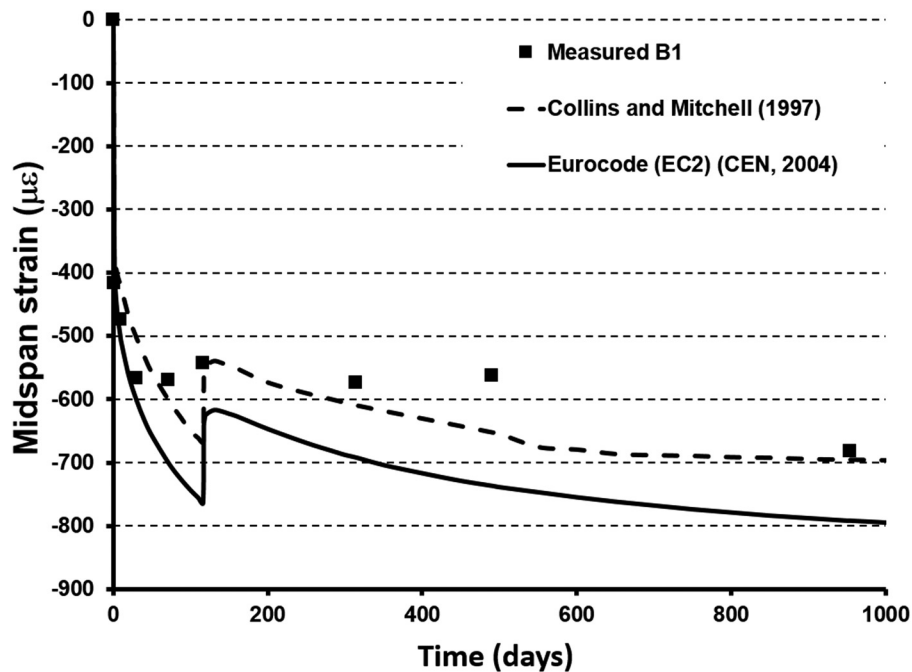
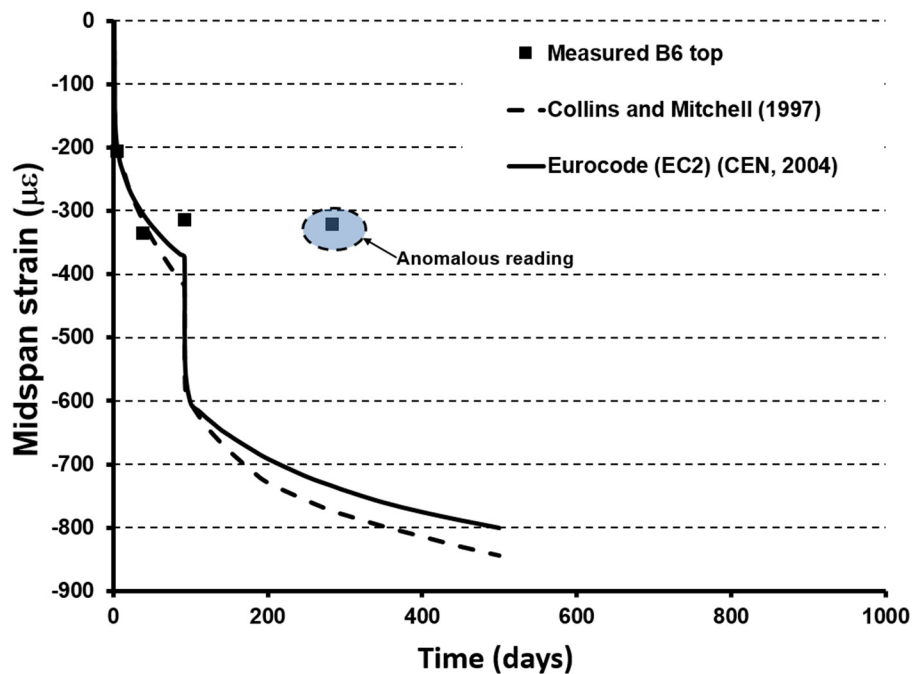**Fig. 14.** Predicted and measured midspan strains for Beam B1 (bottom)

Fig. 15. (Color) Predicted and measured midspan strains for Beam B6 (top)

rupture, causing a loss of compression in the bottom of the concrete beam, then the resulting strains would be around 185 $\mu\varepsilon$, which should be detectable by this system. If continuous monitoring was to be used then the sudden change would likely be noticed, assuming that acceptable data interpretation protocols are followed. It is worth noting that other fiber-optic distributed strain measurement technologies have better accuracy and may be more appropriate for damage detection and assessment depending on the application. For example, Regier and Hoult (2014a) used a Rayleigh backscatter

system to measure strains during a load test of a reinforced concrete bridge and obtained the same level of accuracy as electrical resistance strain gauges. However, even with increased measurement accuracy, long-term damage detection is still a challenge because Regier and Hoult (2014c) demonstrated that a temperature change of just 3°C created the same level of strain change in a bridge as a fully loaded truck. Additionally, one limitation of the Rayleigh system is the length of fiber that can be scanned (maximum 70 m), which may not be enough for some applications. As such, the choice
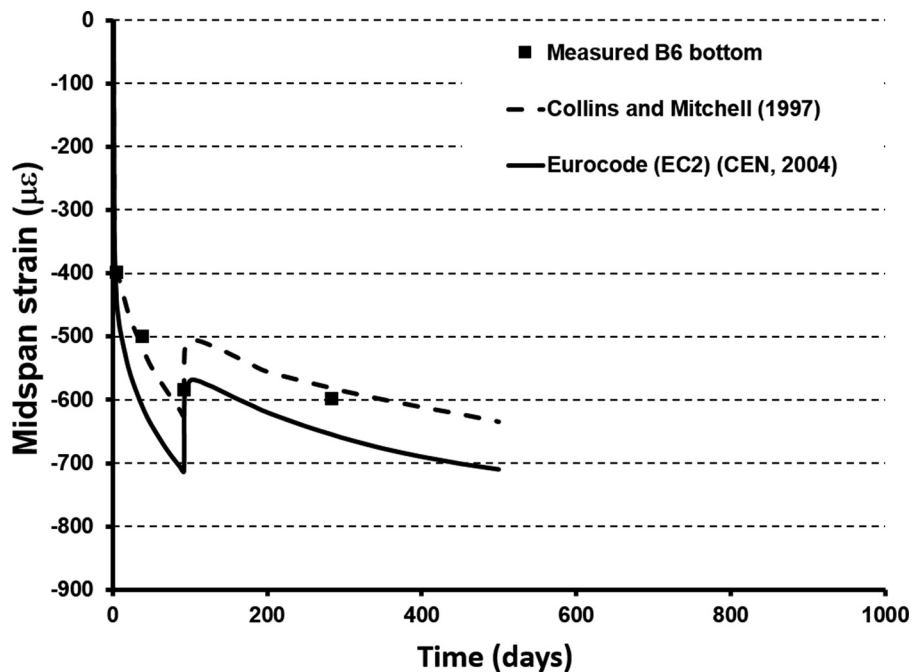
Fig. 16. Predicted and measured midspan strains for Beam B6 (bottom)

of sensor system must be based on a consideration of many parameters to determine the most appropriate system, which may involve some level of compromise.

This monitoring system could also potentially have been used during the construction process to ensure that the prestressing forces applied to the beams were as intended by the designer. Because the technique can provide strain readings along the whole length of a beam, it would have been possible to detect the change in strain distribution, which would have occurred should any of the tendons not have successfully bonded to the concrete.

Conclusions

This research investigated the potential for using a distributed fiber-optic strain measurement system for monitoring prestressed concrete bridges. The low-cost fiber-optic cables used in this research deployment led to a lack of robustness and a gradual loss of monitoring capability over time. This finding is important to note for any similar future monitoring endeavors because it is imperative that monitoring systems can be relied on if decisions are to be taken based on their outputs. It was demonstrated that although the cost of more robust cables is high, the cost of this increased reliability compared to the overall cost of the bridge is relatively small.

It is also important to consider the realistically achievable accuracy of any sensing system prior to its installation to ensure that expected changes to the structure will be distinguishable from sensor noise. Two different empirical prediction models were used for estimating strains due to creep and shrinkage, one from Eurocode 2 (CEN 2004) and one from Collins and Mitchell (1997). The differences between them were smaller in magnitude than the uncertainty in sensor measurements, and the measured data were found to agree reasonably well with both models.

The possibility of using distributed strain sensors to detect local damage was also introduced. Here the accuracy of the system must be selected with respect to the expected level of strain change due to

damage. However, the impact of temperature on long-term measurements must also be accounted for when deciding whether damage detection is practical.

The distributed nature of BOTDR strain measurements is a key benefit for their use in monitoring. Systems such as these have the potential to give a good understanding of the stress state throughout a structure, rather than only at discrete points, as with many alternative sensing technologies. This could prove invaluable for understanding how a structure is behaving, and for detecting problems, both during construction and later in a structure's life.

Data Availability

The following open access data files (Webb et al. 2016), which contain the raw monitoring data, can be downloaded from the University of Cambridge data repository:
- Beam-1-data.xlsx, and
- Beam-6-data.xlsx.

Acknowledgments

Monitoring of Infrastructure; EP/I019308/1, Innovation Knowledge Centre for Smart Infrastructure and Construction; and EP/K000314/1, Innovation and Knowledge Centre for Smart Infrastructure and Construction - Collaborative Programme Tranche 1.

Notation

The following symbols are used in this paper:

A_c = cross-sectional area of the beam;
A_i = area of in situ concrete (deck slab);
A_p = area of precast concrete (beams);
A_s = area of prestressing steel;
$A_s(x)$ = cross-sectional area of the steel tendons effective at a distance x from the end of the beam;
E_c = Young's modulus of the concrete;
E_s = Young's modulus of the steel;
e = eccentricity of the applied prestressing force;
$e(x)$ = eccentricity of the applied prestressing force at a distance x from the end of the beam;
f_{ck} = characteristic concrete cylinder strength;
f_{pk} = characteristic tensile strength of the steel;
I_c = second moment of area of the beam section;
I_i = second moment of area of the in situ concrete deck;
I_p = second moment of area of precast concrete beam;
L = overall length of the beam;
$M(x)$ = the bending moment at a distance x along the beam;
$P_0(x)$ = initial applied prestressing force;
$P_1(x)$ = the force that remains present in the prestressing tendons;
u = length of perimeter exposed to drying;
w = self-weight of the beam per unit length;
x = distance along the length of the beam;
y = distance from the centroid of the beam;
α_a = temperature-induced apparent strain coefficient;
α_f = thermal stain coefficient of embedded fiber;
$\Delta\varepsilon_c$ = mechanical strain change in the concrete;
ΔT = change in temperature;
$\Delta\zeta_s$ = change in raw strain in the strain cable, measured by the analyzer;
$\Delta\zeta_t$ = change in raw strain in the temperature cable, measured by the analyzer;
$\varepsilon(x, y)$ = strain, at a distance x along the length of the beam and a distance y from the centroid; and
$\mu\varepsilon$ = microstrain.

Supplemental Data

Appendices S1–S4, containing detailed calculations, are available online in the ASCE Library (www.ascelibrary.org).

References

Bourne-Webb, P. J., Amatya, B., Soga, K., Amis, T., Davidson, C., and Payne, P. (2009). "Energy pile test at Lambeth College, London: Geotechnical and thermodynamic aspects of pile response to heat cycles." *Géotechnique*, 59(3), 237–248.

Casas, J. R., and Cruz, P. J. (2003). "Fiber optic sensors for bridge monitoring." *J. Bridge Eng.*, 10.1061/(ASCE)1084-0702(2003)8:6(362), 362–373.

CEN (European Committee for Standardization). (2004). "*Eurocode 2: Design of concrete structures-Part 1-1: General rules for buildings.*" *EN 1992-1-1:2004 (E)*, Brussels, Belgium.

Collins, M. P., and Mitchell, D. (1997). *Prestressed concrete structures*, Response Publications, Toronto.

Costa, B. J. A., and Figueiras, J. A. (2012). "Fiber optic based monitoring system applied to a centenary metallic arch bridge: Design and installation." *Eng. Struct.*, 44, 271–280.

Deif, A., Martín-Pérez, B., Cousin, B., Zhang, C., Bao, X., and Lis, W. (2010). "Detection of cracks in a reinforced concrete beam using distributed Brillouin fibre sensors." *Smart Mater. Struct.*, 19(5), 055014.

Gao, J., Shi, B., Zhang, W., and Zhu, H. (2006). "Monitoring the stress of the post-tensioning cable using fiber optic distributed strain sensor." *Measurement*, 39(5), 420–428.

Ge, Y., Elshafie, M. Z. E. B., Dirar, S., and Middleton, C. R. (2014). "The response of embedded strain sensors in concrete beams subjected to thermal loading." *Constr. Build. Mater.*, 70, 279–290.

Gebremichael, Y. M., et al. (2005). "A field deployable, multiplexed Bragg grating sensor system used in extensive highway bridge monitoring evaluation tests." *IEEE Sens. J.*, 5(3), 510–519.

Ghali, A., Gayed, R., and Kroman, J. (2016). "Sustainability of concrete infrastructures." *J. Bridge Eng.*, 10.1061/(ASCE)BE.1943-5592 .0000862, 04016033.

Henault, J. M., et al. (2012). "Quantitative strain measurement and crack detection in RC structures using a truly distributed fiber optic sensing system." *Constr. Build. Mater.*, 37, 916–923.

Hoult, N.A., Ekim, O., and Regier, R. (2014). "Damage/deterioration detection for steel structures using distributed fiber optic strain sensors." *J. Eng. Mech.*, 10.1061/(ASCE)EM.1943-7889.0000812, 04014097.

Hoult, N. A., Bennett, P. J., Middleton, C. R., and Soga, K. (2009). "Distributed fibre optic strain measurements for pervasive monitoring of civil infrastructure." *Proc., 4th Int. Conf. on Structural Health Monitoring of Intelligent Infrastructure (SHMII-4)*, International Society for Structural Health Monitoring of Intelligent Infrastructure, Winnipeg, MB, Canada.

Howells, R. W., Lark, R. J., and Barr, B. I. G. (2005). "A sensitivity study of parameters used in shrinkage and creep prediction models." *Mag. Concr. Res.*, 57(10), 589–602.

Klar, A., et al. (2006). "Distributed strain measurements for pile foundations." *Proc. Inst. Civ. Eng. Geotech. Eng.*, 159(3), 135–144.

Kurashima, T., Horiguchi, T., Izumita, H., Ichi Furkukawa, S., and Koyamada, Y. (1993). "Brillouin optical-fiber time domain reflectometry." *IEICE Trans. Commun.*, E76-B(4), 382–390.

Lark, R. J., Howells, R. W., and Barr, B. I. G. (2004). "Behaviour of post-tensioned concrete box girders." *Proc. Inst. Civ. Eng. Bridge Eng.*, 157(2), 71–81.

Maaskant, R., Alavie, T., Measures, R. M., Tadros, G., Rizkalla, S. H., and Guha-Thakurta, A. (1997). "Fibre-optic Bragg grating sensors for bridge monitoring." *Cem. Concr. Compos.*, 19(1), 21–33.

Matta, F., Bastianini, F., Galati, N., Casadei, P., and Nanni, A. (2008). "Distributed strain measurement in steel bridge with fiber optic sensors: Validation through diagnostic load test." *J. Perform. Constr. Facil.*, 10.1061/(ASCE)0887-3828(2008)22:4(264), 264–273.

Michaud, K., Hoult, N., Lotfy, A., and Lum, P. (2016). "Performance in shear of reinforced concrete slabs containing recycled concrete aggregate." *Mater. Struct.*, 49(10), 4425–4438.

Mohamad, H. (2008). "Distributed optical fibre strain sensing of geotechnical structures." Ph.D. thesis, Univ. of Cambridge, Cambridge, U.K.

Moyo, P., Brownjohn, J. M. W., Suresh, R., and Tijin, S. C. (2005). "Development of fibre Bragg grating sensors for monitoring civil infrastructure." *Eng. Struct.*, 10.1016/j.engstruct.2005.04.023, 27(12), 1828–1834.

Parker, T. R., Farhadiroushan, M., Handerek, V. A., and Rogers, A. J. (1997). "A fully distributed simultaneous strain and temperature sensor using spontaneous Brillouin backscatter." *IEEE Photonics Technol. Lett.*, 9(7), 979–981.

Regier, R., and Hoult, N. A. (2014a). "Distributed strain behavior of a reinforced concrete bridge: Case study." *J. Bridge Eng.*, 10.1061/(ASCE)BE .1943-5592.0000637, 05014007.

Regier R., and Hoult N. A. (2014b). "Concrete deterioration detection using distributed sensors." *Proc. Inst. Civ. Eng. Struct. Build.*, 168(2), 118–126.

Regier, R., and Hoult, N. A. (2014c). "Distributed strain monitoring for bridges: Temperature effects." *SPIE Smart Structures and Materials + Nondestructive Evaluation and Health Monitoring*, International Society for Optics and Photonics, Bellingham, WA.

Vardanega, P. J., Webb, G. T., Fidler, P. R. A., and Middleton, C. R. (2016a). "Assessing the potential value of bridge monitoring systems." *Proc. Inst. Civ. Eng. Bridge Eng.*, 169(2), 126–138.

Vardanega, P. J., Webb, G. T., Fidler, P. R. A., and Middleton, C. R. (2016b). "Bridge monitoring." *Innovative bridge design handbook: Construction, rehabilitation and maintenance*, A. Pipinato, ed., Butterworth Heinemann, Oxford, U.K., 759–775.

Villalba, S., and Casas, J. R. (2013). "Application of optical fiber distributed sensing to health monitoring of concrete structures." *Mech. Syst. Sig. Process.*, 39(1–2), 441–451.

Wang, Y., and Huang, H. (2011). "Optical fiber corrosion sensor based on laser light reflection." *Smart Mater. Struct.*, 20(8), 085003.

Webb, G. T., Vardanega, P. J., Fidler, P. R., and Middleton, C. R. (2014a). "Analysis of structural health monitoring data from Hammersmith flyover." *J. Bridge Eng.*, 10.1061/(ASCE)BE.1943-5592.0000587, 05014003.

Webb, G. T., Vardanega, P. J., and Middleton, C. R. (2014b). "Categories of SHM deployments: Technologies and capabilities." *J. Bridge Eng.*, 10.1061/(ASCE)BE.1943-5592.0000735, 04014118.

Webb, G. T. (2010). "Structural health monitoring of bridges." M.Eng. thesis, Univ. of Cambridge, Cambridge, U.K.

Webb, G. T. (2014). "Structural health monitoring of bridges." Ph.D. thesis, Univ. of Cambridge, Cambridge, U.K.

Webb, G. T., Vardanega, P. J., Hoult, N. A., Fidler, P. R., Bennett, P. J., and Middleton, C. R. (2016). "Research data supporting 'Analysis of fiber-optic strain-monitoring data from a prestressed concrete bridge.'" ⟨http://doi.org/10.17863/CAM.55⟩.

Whelan, M. J., Gangone, M. V., Janoyan, K. D., Hoult, N. A., Middleton, C. R., and Soga, K. (2010). "Wireless operational modal analysis of a multi-span prestressed concrete bridge for structural identification." *Smart Struct. Syst.*, 6(5–6), 579–593.

Zhang, W., Shi, B., Zhang, Y. F., Liu, J., and Zhu, Y. Q. (2007). "The strain field method for structural damage identification using Brillouin optical fiber sensing." *Smart Mater. Struct.*, 16(3), 843–850.

Zhou, Z., Chen, G., and Ou, J. (2009). "Long-term monitoring of steel strand prestress loss by using FRP-OFS." *Proc., 4th Int. Conf. on Structural Health Monitoring of Intelligent Infrastructure (SHMII-4)*, International Society for Structural Health Monitoring of Intelligent Infrastructure, Winnipeg, MB, Canada.